Describing magnetorheology under a colloidal glass approach

J. P. Segovia-Gutiérrez,[1] J. de Vicente,[1] Antonio M. Puertas,[2,*] and R. Hidalgo-Alvarez[1]
[1]*Department of Applied Physics, Faculty of Sciences, University of Granada, Fuentenueva s/n, 18071-Granada, Spain*
[2]*Group of Complex Fluids Physics, Department of Applied Physics, University of Almeria, 04120 Almería, Spain*
(Received 1 March 2017; revised manuscript received 5 April 2017; published 1 May 2017)

The equilibrium structure and dynamics of magnetorheological (MR) fluids are studied in this work by simulations, where particles are modeled as dipoles with a quasihard spherical core. Upon increasing the interaction strength, controlled experimentally by the magnetic field, elongated clusters grow and, for intense fields, thick columns form, aligned with the field. The dynamics of the system is monitored by the mean-squared displacement and density correlation functions, which show an increasing slowing down with the attraction strength. The correlation function shows a two-step decay, with a separation between microscopic and long time dynamics, a typical hallmark of undercooled fluids. We have therefore analyzed the dynamics of this MR fluid using the typical concepts for undercooled fluids. Thus, the second decay of the density correlation function is fitted with a stretched exponential, and the wave-vector dependence of the fitting parameters studied. Both the amplitude and the time scale oscillate in phase with the structure factor. Our results support the idea that the magnetorheological effect is in fact the manifestation of a colloidal system approaching an attractive glass transition (or gel transition).

DOI: 10.1103/PhysRevE.95.052601

I. INTRODUCTION

Externally controllable materials are of outstanding interest in materials science, and in particular, in soft matter. Within this specific frame, magnetorheological (MR) fluids deserve special attention because their rheological properties can be controlled by an external magnetic field [1]. Due to this noninvasive simple control, MR fluids have been used in many different applications, even before a full understanding of the physics involved was reached. Although MR fluids appeared on the scientific stage around 1950 [2–4], applications in new technology are still developing [5], involving the use of magnetic fields to control the thermal energy transfer [6,7], biomedicine [8], precision polishing [9–11], sound propagation [12], isothermal magnetic advection [13], and chemical sensing [14–16], among others.

Conventional MR fluids consist in two phases: (i) a solid or disperse phase comprised of magnetizable microparticles, and (ii) a continuous phase (bulk), where particles are dispersed [1]. When an external magnetic field is applied, particles are magnetized and behave as magnetic dipoles (in a first approximation). Experiments and early simulations [17–20] have shown that linear aggregates of particles form, aligned in the direction of the magnetic field, leading to columnar aggregates at intense fields. This provokes an important increase in the system viscosity that can be of several orders of magnitude. If the magnetic field exceeds a certain strength, a threshold stress is observed, the so-called yield stress, to make the system flow and viscoelasticity comes up [21]. This overall phenomenology is known as the MR effect and it depends not only on the magnetic field intensity, but also on the particle concentration, the dimensions, morphology, or material of particles [22]. However, most studies have focused on the out-of-equilibrium and nonlinear regime, where the system is subject to external stresses.

The dramatic increase of the shear viscosity and development of an elastic behavior is common also to the glass transition [23]. In colloids, two different glass transitions have been identified: the so-called repulsion-driven glass transition, induced by the increase of the particle concentration, which is similar to the glass transition in atoms or molecules, and an attraction-driven glass transition [24,25], which is connected to structure formation and gels [26]. Anisotropic interactions and multibody interactions, have also been used to produce gel formation, but the overall phenomenology is similar to the attraction-driven glass transition, extended to much lower densities [27,28]. Upon increasing the attraction strength, e.g., in colloid-polymer mixtures, an intricate percolating structure forms, provoking a slowing down of the structural relaxation, and ultimately viscoelastic behavior. Note that, whereas the repulsion-driven glass transition takes place in a system with liquidlike structure (i.e., without long-range structure), the attractive one is observed in a structurally heterogeneous system. Closer to magnetorheological fluids, dipolar fluids have been studied by simulations, showing structure formation (very similar to gels) together with an important dynamic slowing down, when the temperature is lowered [29,30]. Motivated by this analogy, we try to rationalize in this work the MR effect as a dynamic-arrest transition induced by the external magnetic field.

We present here a simulation study, focused on both the equilibrium structure and dynamics of a MR fluid. A polydisperse system is used to avoid crystallization, which would provoke a sudden arrest of the dynamics, as in isotropic fluids. We have shown previously that polydispersity effectively impedes crystallization, and the system develops viscoelastic behavior continuously, as shown by the shear and elastic moduli [31]. In this work, we concentrate on the dynamics of the system, which is monitored with the mean-squared displacement and density correlation functions, measured with wave vectors parallel and perpendicular to the external field, and correlate with it the structure of the system. All states studied here are equilibrated. For strong

*apuertas@ual.es

interactions, large aggregates of particles form (columns), and the correlation function decays in two steps. The wave vector dependence of the long-time decay, signaling the structural relaxation, is analyzed, which allows us to identify the modes or length scales where relaxation is more hindered. The long-time structural decay can be fitted with a stretched exponential, and the amplitude and relaxation time oscillate in phase with the structure factor, as in undercooled fluids. Finally, we study the dynamical heterogeneities, another hallmark of undercooled fluids [32]. Our MR fluid displays a maximal non-Gaussian behavior in the time range between the microscopic and structural relaxations, in agreement with conventional undercooled fluids.

II. SIMULATION DETAILS

Simulations are run with microscopic Brownian dynamics, mimicked by using the Langevin equation, namely, damped Newtonian dynamics. For particle i, the Langevin equation reads:

$$m_i\ddot{\mathbf{r}}_i = \sum_j \mathbf{F}_{ij} - \gamma_i\dot{\mathbf{r}}_i + \mathbf{f}_i, \tag{1}$$

where m_i and γ_i are the particle mass and friction coefficient with the solvent, $\mathbf{F}_{ij}$ is the interaction force between particles i and j, and $\mathbf{f}_i$ is the Brownian force, which is linked to the friction force by the fluctuation-dissipation relation: $\langle \mathbf{f}_i(t)\mathbf{f}_j(t')\rangle = 6k_BT\gamma\delta(t-t')\delta_{ij}$, where k_BT is the thermal energy, and $\delta(x)$ and δ_{ij} are the Dirac-δ function and the Kronecker delta, respectively. Note that in the Langevin model, the short-time dynamics is ballistic due to the inertial term, left-hand side of Eq. (1), while experimental colloids follow real Brownian dynamics, although the Brownian motion can be hardly observable for large particles. In any case, Langevin or Brownian dynamics resolve the microscopic and structural dynamics, that, as shown below, is in the center of the analysis of our results.

The particle-particle interaction contains two terms: a dipolar term and a core-core repulsion. The dipolar force is given by:

$$\mathbf{F}_{ij}^{\mathrm{mag}} = 3U_0\left(\frac{1}{|\mathbf{r}_{ij}|}\right)^4 [(2\,\cos^2\theta_{ij} - \sin^2\theta_{ij})\widehat{r} + \sin 2\theta_{ij}\widehat{\theta}], \tag{2}$$

where $\mathbf{r}_{ij}$ denotes the relative position vector between two particles and θ_{ij} is the angle that $\mathbf{r}_{ij}$ forms with the magnetic field direction, $\widehat{r}$ and $\widehat{\theta}$ represent the unit vectors in the direction defined by the pair of particles and the angular vector, respectively. The parameter U_0 sets the strength of the attraction and is given by the physical parameters of the system. Under the linear magnetization approximation, and in the absence of many-body effects, $U_0 = 4\pi\mu_0\mu_{\mathrm{cr}}\beta^2 a_i^3 a_j^3 H_0^2$, where H_0 is the modulus of the external magnetic field strength, μ_0 is the magnetic permeability of the vacuum, $\mu_{\mathrm{cr}} = \frac{\mu_c}{\mu_0} \sim 1$ refers to the relative magnetic permeability of the continuous phase and β is the contrast factor, $\beta = (\mu_p - \mu_c)/(\mu_p + 2\mu_c)$, with μ_c and μ_p the magnetic permeabilities of the continuous medium and particles, respectively. Finally, a_i and a_j are the radii of the interacting particles. Note that the range of the dipolar interaction is longer than other conventional interaction potentials. Thus, we have not used neighbor lists to speed up the calculation of the interactions.

The core-core repulsion has an exponential form:

$$\mathbf{F}_{ij}^{\mathrm{rep}} = -\frac{3U_0}{16a^4}\exp\left(-100\frac{|\mathbf{r}_{ij}| - (a_i + a_j)}{a_i + a_j}\right)\widehat{r}, \tag{3}$$

which is continuous and describes correctly the lateral attractive interaction between columns, given its short range [17,33]. Note that the core-core repulsion is proportional to U_0, in order to make the total potential (or force) proportional to U_0. In this way, only the intensity of the potential depends on U_0, but not its shape, which is expected to be closer to experimental systems. The minimum of the interaction potential is at $1.986a$ (taking $a_i = a_j = a$), independent of U_0, while it shifts from this value for $U_0 = 1k_BT$ to $r_{\mathrm{min}} = 1.900$ for $U_0 = 60\,k_BT$, if the dependence on U_0 is not included. To simulate hard spheres, U_0 is set to zero in the magnetic interaction, but $U_0 = 1k_BT$ in the core repulsion. Our system is different from standard dipolar fluids [29,30] because the magnetic dipolar moment depends on the external field, and is always oriented parallel to it.

$N = 1000$ particles are simulated in a cubic box with periodic boundary conditions. To avoid crystallization of the system a polydisperse system is considered, mimicking experimental MR fluids, although the size distribution is much simpler in the simulated system. A flat distribution of radii of width $\Delta = 0.2a$, being a the average radius, is used. Accordingly, the particle mass is calculated as $m_i = m_0(a_i/a)^3$, and the friction coefficient as $\gamma_i = \gamma_0 a_i/a$. Lengths are measured in units of the mean radius, a, energy in units of k_BT, m_0 is set to 1 and the damping coefficient γ_0 is chosen as $10\sqrt{k_BTm_0}/a$, in these dimensionless units. The equations of motion were integrated following Heun's algorithm [34] with a time step of $\delta t = 0.0005a\sqrt{m/k_BT}$. A fixed volume fraction is used, set to 5% (this concentration is lower than the typical experimental one, but allows us to identify the slowing down due to clustering of particles). The external field is oriented along the z axis. The orientational order parameter Q_6 introduced by Steinhardt *et al.* [35] was used to monitor the crystallization of the system. This showed that the size distribution used here is enough to avoid crystallization [31].

III. RESULTS

At low particle concentration, the system evolves from a gas state to form elongated transient clusters upon increasing the interaction strength, U_0, with the clusters oriented along the field direction. Larger values of U_0 provoke further clustering, resulting in long thick columns that span through the system in the direction of the external field. The dynamics of the system therefore becomes progressively slower, as the diffusion in large clusters is slower, increasing the viscosity and ultimately arrests (ideally) if the bonds are strong enough to trap the particles permanently [36,37].

If a monodisperse system is used, crystalline order within the columns appears with a body-centered-tetragonal structure [38–42], which is the ground-state structure of both electrorheological and MR fluids. This transition is also noted in the dynamics by a sharp decrease of particle diffusion,

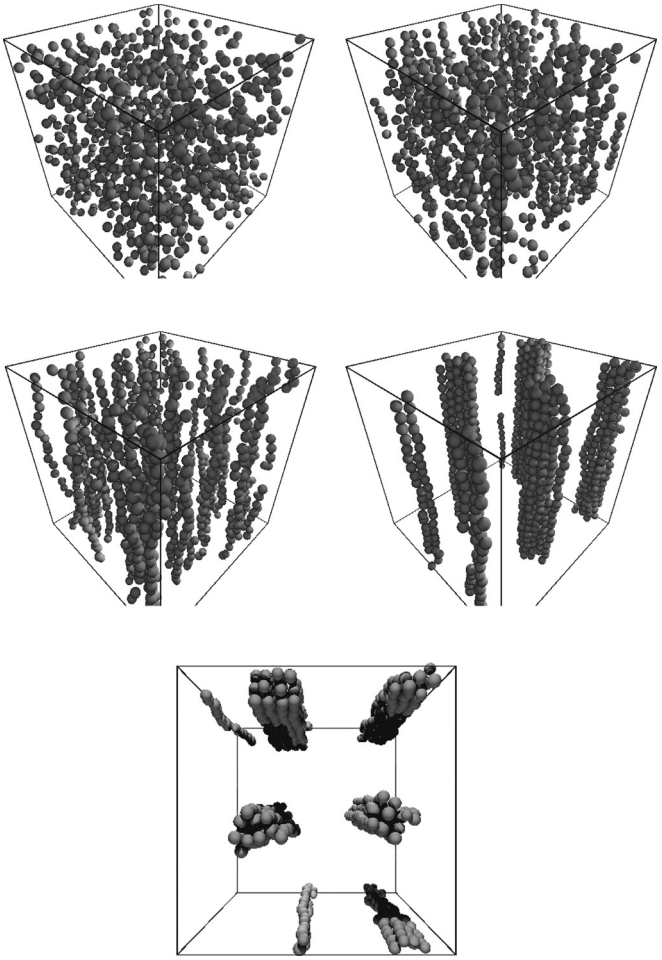

FIG. 1. Snapshots of the simulation for different values of U_0. The magnetic field is applied in the vertical direction, except in the lowest snapshot where it is perpendicular to the plane of the image. From the top left to the bottom right: hard spheres; $U_0 = 0k_BT$ $U_0 = 25k_BT$; $U_0 = 35k_BT$; $U_0 = 60k_BT$; top view of $U_0 = 60k_BT$ in the lower snapshot.

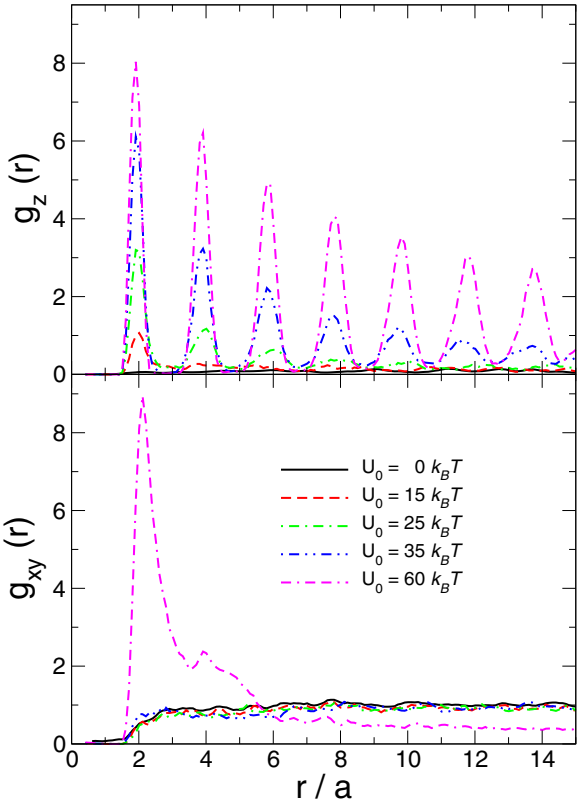

FIG. 2. Parallel and perpendicular components of the pair correlation function (top and bottom, respectively), for different values of U_0, as labeled. Recall that $U_0 = 0$ corresponds to hard spheres.

indicating the solidification of the system. We are not, however, interested in this, and thus a polydisperse system is used to observe a gradual solidification of the system upon increasing the strength of the dipolar interaction U_0 [31]. We expect that the particular shape of the size distribution does not affect the results qualitatively.

A. Structure

We focus first on the structure of the system for increasing U_0. Different snapshots of the system are presented in Fig. 1, showing the formation of clusters, weak chains, and thick columns. It must be mentioned that, by visual inspection of the evolution of the system in the simulation, all of these structures are transient. For $U_0 = 0$ (recall that the core repulsion is always present) the system is completely disordered; when $U_0 = 25k_BT$ we can hardly distinguish small aggregates, which contain a small number of particles; clear elongated thin structures are observed at $U_0 = 35k_BT$; finally, at the highest value of U_0, $60k_BT$, thicker aggregates are formed along the magnetic field direction. This visual evolution highlights the importance of lateral chain aggregation and reveals a structural disorder even at high values of U_0, indicating that polydispersity indeed prevents crystallization. This evolution is in agreement with previous results in the literature, showing the formation of elongated clusters and columns in MR fluids [36,37]. On the other hand, in dipolar fluids an intricate network forms upon lowering the temperature, but they align only when an intense external field is present [30].

The structure is studied quantitatively using the pair distribution functions, $g(\mathbf{r})$, and structure factors, $S(\mathbf{q})$, taking into account the anisotropy of the system. For $g(\mathbf{r})$, the component parallel to the field is calculated considering only the pairs of particles closer than one radius when projected onto the plane perpendicular to the field. For the perpendicular component, only pairs with a distance smaller than one radius in the field direction are accounted for. These restrictions affect the total number of pairs of particles, so that the distribution functions do not show the limit $g(r \to \infty) \to 1$.

Figure 2 shows the pair distribution function, $g(\mathbf{r})$, along the directions parallel to the external field (top panel) and perpendicular (bottom panel). Increasing the field strength, U_0, induces quasi-long-range order in the direction of the field, but almost no correlation in the perpendicular direction. This indicates the formation of elongated clusters or chains aligned with the external field, as shown by the smeared peaks at multiples of $2a$ that grow when U_0 increases (these peaks are not sharp due to the size polydispersity [31]), and the absence of peaks in the perpendicular direction. Only for the

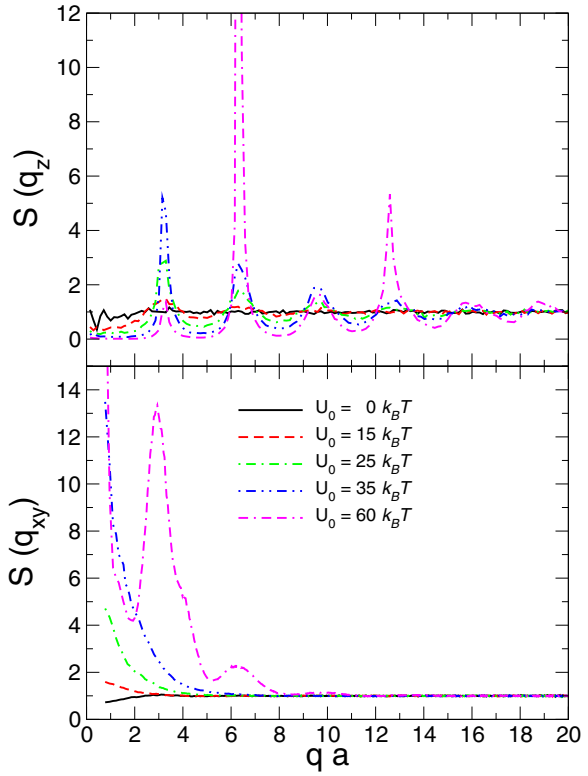

FIG. 3. Static structure factor for different values of U_0 as labeled with a wave vector parallel and perpendicular to the external field (top and bottom, respectively). Recall that $U_0 = 0$ corresponds to hard spheres.

highest value of U_0 studied, $U_0 = 60k_BT$, the perpendicular component of $g(\mathbf{r})$ shows a peak at $r = 2a$, and a tail extending to long distance, reflecting the lateral aggregation of the chains to form thick columns of several particles in diameter.

The static structure factor is studied next, to establish a connection with experimental scattering techniques. In this case, the anisotropy of the system is captured by the direction of the wave vector, $\mathbf{q}$. The structure factor, $S(\mathbf{q})$, is defined as:

$$S(\mathbf{q}) = \langle \rho(\mathbf{q})\rho^*(\mathbf{q}) \rangle = \frac{1}{N} \left\langle \sum_{j,k} e^{i\mathbf{q}\cdot(\mathbf{r}_j - \mathbf{r}_k)} \right\rangle, \qquad (4)$$

where the sum runs over all pairs of particles in the system and the average implies ensemble averaging. Contrary to the calculation of $g(\mathbf{r})$, all pairs of particles are considered, without restriction, but the direction of $\mathbf{q}$ is set.

The results are shown in Fig. 3 for $\mathbf{q}$ vectors parallel and perpendicular to the external field, and the same values of U_0 as previous figures. In the parallel component, the system is almost uncorrelated, $S(q) = 1$, for $U_0 = 0$, and develops pronounced oscillations as the particles cluster. It is interesting to note that the most prominent peak is found for the highest U_0 at $qa \approx 2\pi$, corresponding to a distance of one radius approximately, contributed by the pairs of particles separated by this distance but also by the corresponding Fourier component of the pairs separated $2a$, which are dominant (as shown in the pair distribution function). The pairs separated by a distance of one radius (in the field direction) correspond to particles in neighboring columns, arranged with a mismatch of one radius, to minimize the energy. Note that this peak surpasses the first neighbor peak only when thick columns of particles form, induced by the lateral attraction between columns. The structure factor in the low-q region decreases with increasing U_0, indicating that the system is less compressible (in this direction) by the formation of vertically aligned structures.

The structure factor for wave vectors perpendicular to the external field, on the other hand, shows a very different behavior with a rise in the low-q region as the main feature, and oscillations only for high U_0. This indicates the depletion of particles in the plane perpendicular to the field, and the lateral aggregation of columns at high U_0. In this case, side-by-side chains of particles separated by $2a$, but shift one radius in the z direction (as required by the BCT-like structure), is the main contribution to the dominant peak at $qa \approx \pi$. The overall shape of the structure factor in this $\mathbf{q}$ direction is strongly reminiscent of colloidal gels, where a low-q peak develops due to the heterogeneous structure and grows with the attraction strength. This peak increases and moves to smaller wave vectors as the attraction increases, until it arrests at the gel transition.

B. Dynamics

We move now to the study of the dynamics of the system. Let us recall that our simulations follow Langevin dynamics microscopically, i.e., with friction and random forces explicitly included, in addition to the interaction and external forces, and short-time ballistic dynamics. As shown previously, denser structures form when the external magnetic field increases, which is expected to hinder particle diffusion. This is confirmed by studying the mean-squared displacement (MSD), shown in Fig. 4 in the direction of the external field (top panel) and transversal plane (bottom panel). This reveals the slowing down of the system upon increasing U_0—the MSD develops an intermediate subdiffusive regime between the short-time dynamics and long-time diffusion, indicative of a transient trapping of the particles at a particular length. Note, however, that this intermediate regime is different in the field direction (Z axis) and the transversal plane (XY plane), with a shorter localization length in the former than in the latter. Similar differences have been reported in dipolar fluids when an external field (intense enough to align the clusters) is applied [30]. In undercooled fluids and colloidal glasses and gels, a similar separation between microscopic dynamics and long-time diffusion is observed, which grows upon approaching the glass or gel transition. At the transition point, long-time diffusion is suppressed and the MSD arrests at a finite length, known as localization length. It is also worth mentioning that although Langevin dynamics is ballistic at short times, in contrast with Brownian dynamics followed by real colloids, the increasing separation between microscopic and structural relaxations is independent of the microscopic dynamics, as shown previously for glasses [43,44].

The self-diffusion coefficient, obtained from the long-time behavior of the MSD, is, nevertheless, very similar in both the direction of the external field and perpendicular to it, as shown in Fig. 5 (although the diffusion coefficient in the transversal plane is systematically slightly larger). This indicates that the

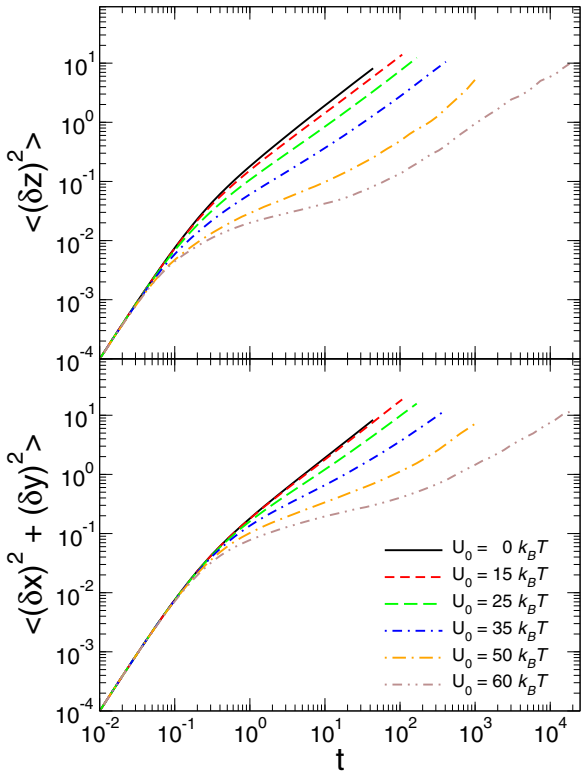

FIG. 4. Mean-squared displacements in the z direction (top) and xy plane (bottom) for different interaction strengths, as labeled.

trapping mechanism is only one, namely, once the particle can diffuse in one direction, it diffuses in all directions. Interestingly, the diffusion coefficient can be fitted by an Arrhenius form $D\gamma_0 \propto \exp\{-AU_0/k_BT\}$, with $A = 0.106$, i.e., an activation energy $U_0^* \approx 9.5k_BT$. This behavior starts when large elongated aggregates form, and continues for increasing U_0, even when particles form thick columns.

This behavior is strongly similar to that of supercooled liquids or glasses, and more particularly, of colloidal gels.

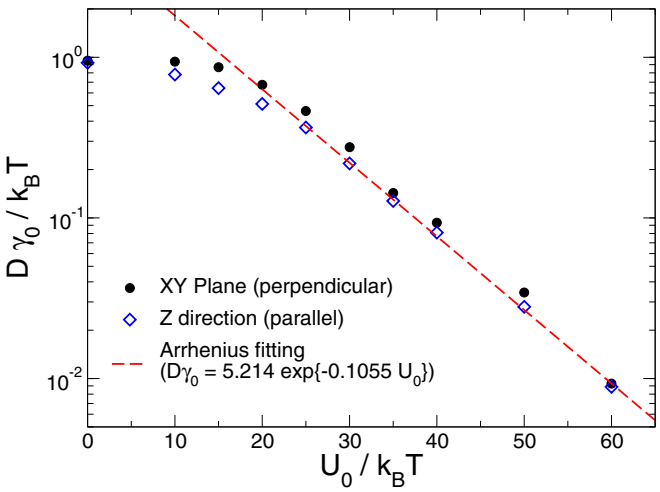

FIG. 5. Longitudinal and transversal diffusion coefficients as a function of U_0. The discontinuous line shows the Arrhenius fitting to the data at larger U_0.

There, a spherical attraction of low or moderate strength induces reversible bonds between the particles, forming a long-lived network, spanning in all three directions with a low density of particles, and with a structural relaxation time that increases with the attraction strength [45]. The dynamics of this system is similar to that of glasses, and in fact, both of them have been described with mode coupling theory, particularly of dense gels [24,25]. Our system, also forms equilibrium supraparticle structures with an overall low particle density and large relaxation times, although the anisotropy of the interaction makes them percolate in only one direction (set by the external field). The dynamics of the system, as monitored by the MSD, shows the typical shape of undercooled fluids, with the transient trapping extending over longer times as the glass is approached, until the trapping becomes permanent (ideally) beyond the glass transition. In our case, however, the Arrhenius behavior would indicate a continuous slowing down of the dynamics without a glass transition, probably due to the inefficient trapping of the particles in the lateral direction.

While the MSD shown above studies the single-particle dynamics, it is also convenient to study the intermediate scattering function or density correlation function, defined as:

$$\Phi_q(t) = \frac{1}{N}\left\langle \sum_{j,k} e^{i\mathbf{q}\cdot(\mathbf{r}_j(t)-\mathbf{r}_k(0))} \right\rangle, \tag{5}$$

which measures the overall structural relaxation of the system, and fulfills $\Phi_q(t=0) = S(q)$. Figures 6 and 7 show the normalized intermediate scattering function for different states and wave vectors parallel and perpendicular to the external field, respectively. Although the parallel component shows a nontrivial behavior with the wave vector, both components show that the structure relaxes completely for all wave vectors, i.e., $\Phi_q(t \to \infty) \to 0$, confirming that the columns shown in the snapshots above are transient and will dissolve completely for long enough times. In general, it is observable that the relaxation time increases with U_0, as expected from the single-particle dynamics.

Following the analogy with supercooled fluids, we have fitted the long-time decay of $\Phi_q(t)$ for the state with U_0 with the Kohlrausch-Williams-Watt (KWW) form,

$$\Phi_q(t) = A_q e^{-(t/\tau_q)^{\beta_q}}, \tag{6}$$

which is typically used for the analysis of glasses and gels. This form results from the sum of many exponential decays weighted by some distribution of individual relaxation times, with β_q controlling the width of this distribution. Typically, $\beta_q < 1$, signaling a wide distribution of relaxation times, resulting in a stretched exponential decay in $\Phi_q(t)$. The dashed lines in Figs. 6 and 7 show the fittings for different wave vectors. Indeed, the final decay of $\Phi_q(t)$ can be properly described by this form, with acceptable accuracy. Stretched exponentials are found in all cases.

This functional form is used to analyze the wave-vector dependence of $\Phi_q(t)$, for both $\mathbf{q}$ parallel and perpendicular to the magnetic field (for all wave vectors, the correlation functions have been fitted for $t > 5$, describing the structural long-time decay). The fitting parameters A_q and τ_q are shown in Fig. 8 in the top and bottom panel, respectively, with the structure factor for $\mathbf{q}$ parallel to the field. The top panel

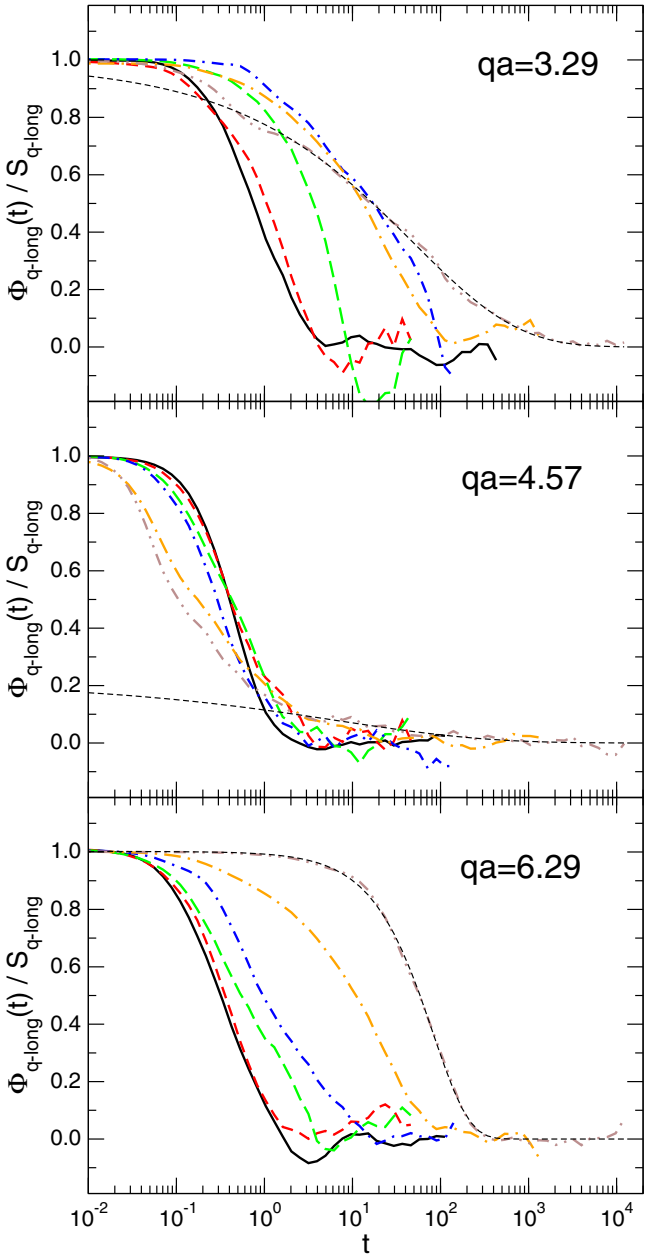

FIG. 6. Normalized density correlation function for three wave vectors parallel to the magnetic field, as labeled. Different values of U_0, with the same code as Fig. 4 are shown. The dashed line shows the KWW fitting to the final decay for the state with $U_0 = 60k_BT$.

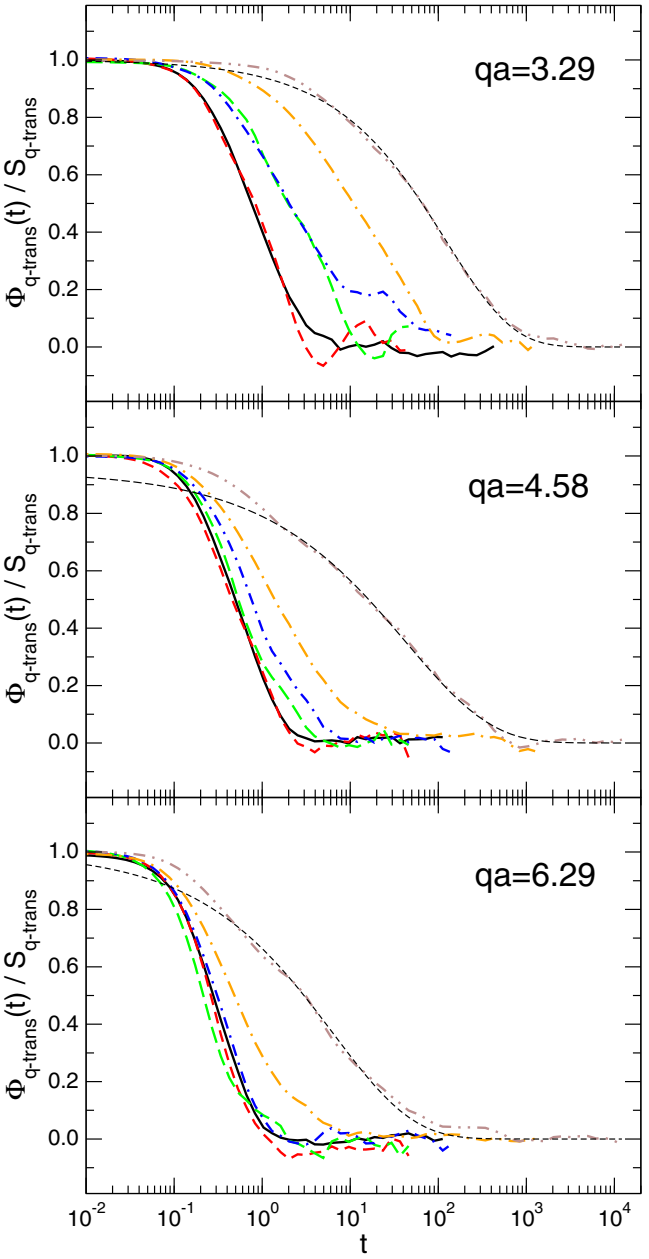

FIG. 7. Normalized density correlation function for three wave vectors perpendicular to the magnetic field, as labeled. Different values of U_0, with the same code as Fig. 4 are shown. The dashed line shows the KWW fitting to the final decay for the state with $U_0 = 60k_BT$.

highlights the strong oscillations of A_q, resulting in the nontrivial behavior observed in Fig. 6. More interestingly, A_q oscillates in phase with the structure factor, indicating that the structure is responsible for the dynamic slowing down. At low wave vectors, the amplitude raises due to the polydispersity of the system, which freezes the mixing of different species [46]. The time scale, τ_q, shows an overall hydrodynamic q^{-2} behavior, with oscillations related to the structure factor.

The intermediate scattering functions for **q** perpendicular to the external field can be described with $A_q \approx 1$ for wave vectors up to $qa \sim 8$ (where the statistics becomes problematic), as shown by the fittings in Fig. 7. This result is somewhat unexpected, as the localization length is larger than in the parallel case, which should produce smaller values of A_q. Note, however, that the MSD measures the dynamics of single particles, while the density correlation function monitors the structural relaxation. The difference between both results, indicates the importance of collective motion (such as motion in clusters, branches, or breath modes). The time scale, on the other hand, follows the expected q^{-2} trend, and oscillates in phase with the structure factor for q perpendicular to the field, as shown in Fig. 9.

The single-particle dynamics can be also studied with the self part of the density correlation function, taking $j = k$ in the

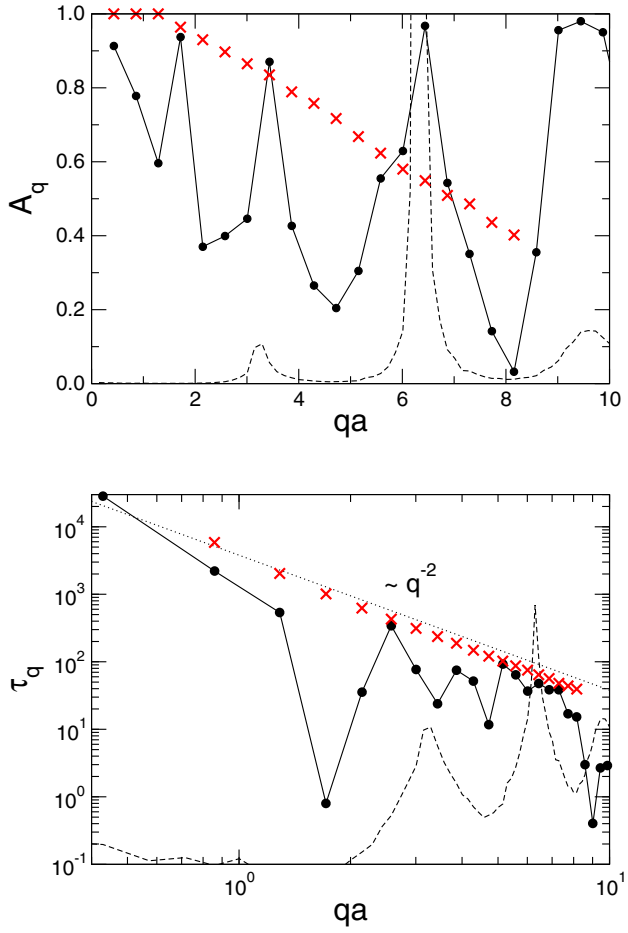

FIG. 8. Parameters from the KWW fitting to the density correlation functions, and its self part, of the state with $U_0 = 60k_BT$ for $\mathbf{q}$ parallel to the external field: Amplitude A_q (top) and time scale τ_q (bottom). Both of them are compared with the structure factor for q parallel (dashed line). The black circles represent the data for the global correlation function and the crosses for its self part.

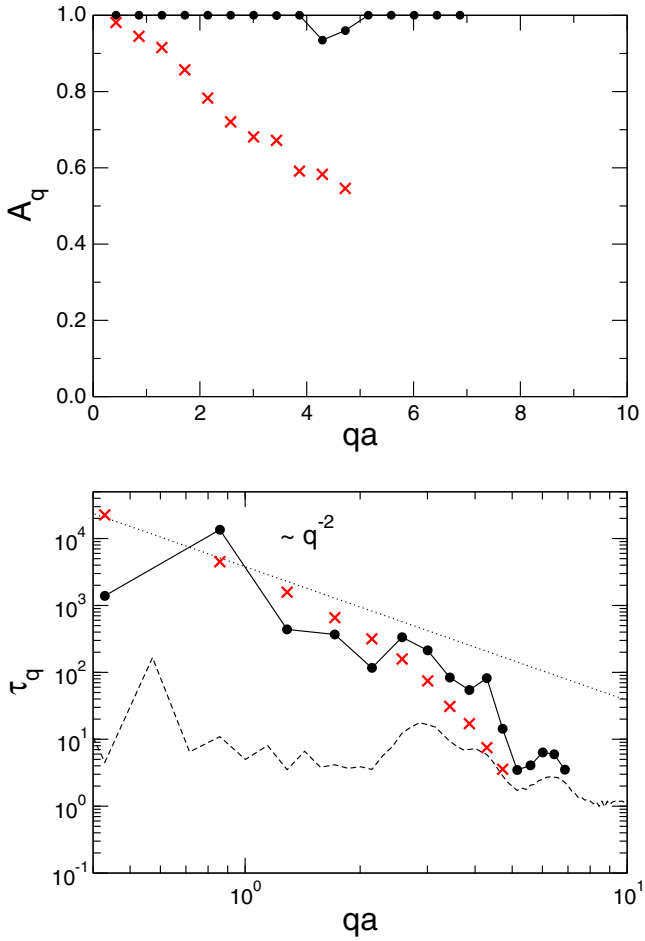

FIG. 9. Same as Fig. 8, for $\mathbf{q}$ perpendicular to the external field.

summation in Eq. (5). The resulting correlation function shows also a two-step decay, as the global function, and the second decay can be fitted with the KWW stretched exponential. The fitting parameters, characterizing the single-particle dynamics, are included also in Figs. 8 and 9 (the same time range is used in the fittings as in the total correlation function, $t > 5$, for all wave vectors). The results indicate that particles move mainly in clusters in the longitudinal direction (as indicated by the $\tau_q^s \sim q^{-2}$ behavior) and confirm the important decoupling between self-particle motion and structural motion in the transversal plane, although the time scales evolve similarly (Fig. 9).

Finally, we study another characteristic signature of colloidal glasses and gels, namely, the dynamical heterogeneities of the system. This is normally studied using the non-Gaussian parameter, α_2, that measures the deviation of the distribution of displacements from the Gaussian shape. In the isotropic case, this is given by:

$$\alpha_2 = \frac{3\langle \delta r^4(t)\rangle}{5\langle \delta r^2\rangle^2} - 1 \qquad (7)$$

and it is zero for a Gaussian distribution of displacements. In supercooled fluids, α_2 starts from zero at $t = 0$, and describes a maximum to tend to zero again at long times; the height of the maximum grows as the glass transition is approached, and its typical times correlate with the structural relaxation time.

In our case, the definition of α_2 is slightly modified to measure the distribution in the directions parallel and perpendicular to the field; $\alpha_{2,z} = \langle \delta z^4(t)\rangle/3\langle \delta z^2\rangle^2 - 1$, and similar definitions for the transversal directions. Figure 10 shows the non-Gaussian parameter in both directions, for different states increasing U_0. Again the qualitative behavior of this parameter is similar to that of supercooled fluids, showing strong deviations from the Gaussian distribution in the time range when the particles are transiently trapped. In agreement with the MSD in Fig. 4, the particles are more tightly caged in the direction of the magnetic field (smaller localization lengths and larger non-Gaussian parameters), but the trapping extends over larger time intervals in the perpendicular plane (longer plateaus and wider peaks). The escape from this cage recovers the Gaussian distribution in the particle displacement in both directions.

While these dynamical heterogeneities are present in all glasses, in colloidal gels they are increased by the structural heterogeneity of the system. In fact, different populations of particles with different mobilities have been identified [47], due to the structural heterogeneity of the system—the particles

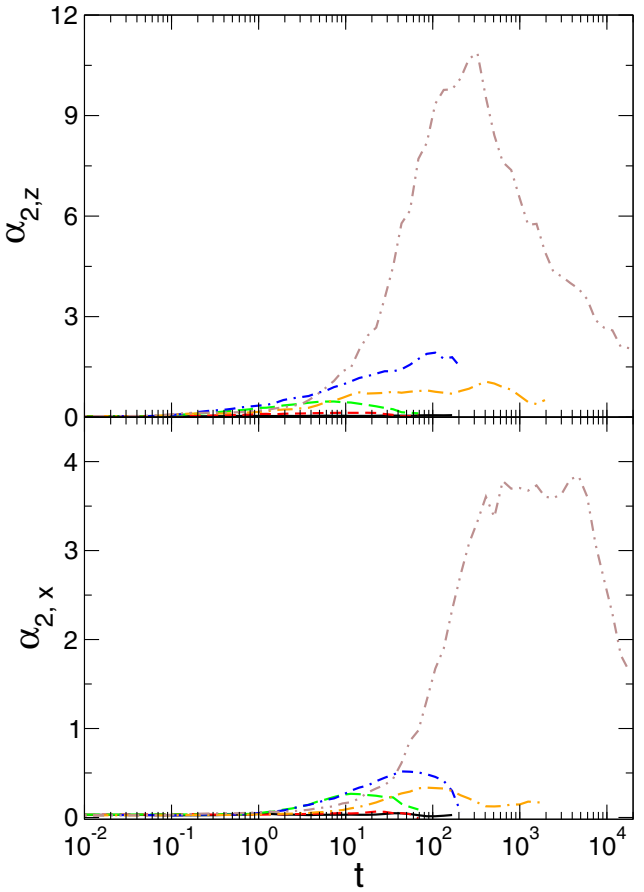

FIG. 10. Non-Gaussian parameter for the displacement in the longitudinal direction (top) and transversal (bottom), as a function of time, with the same code as Fig. 4.

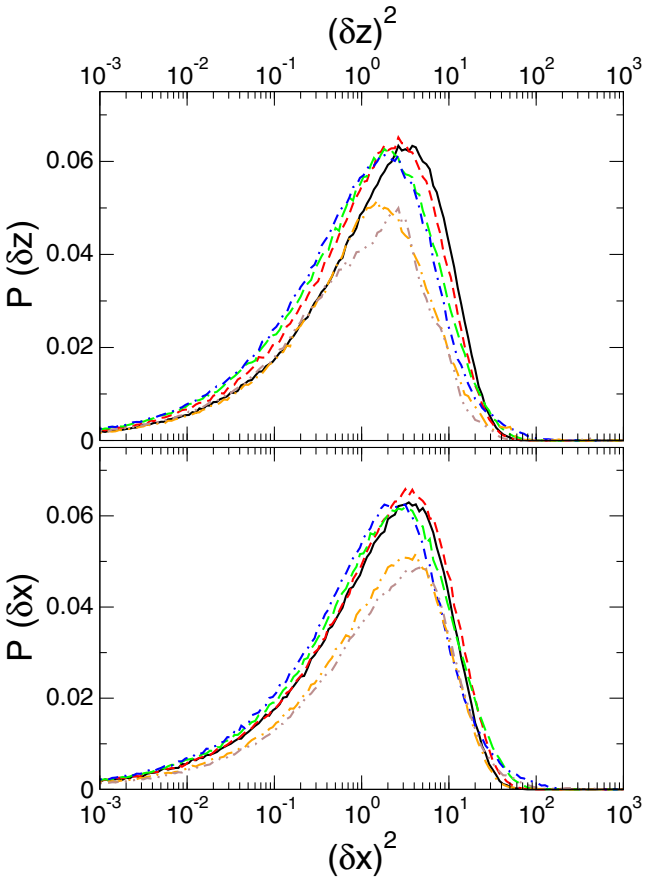

FIG. 11. Particle displacement distribution in the direction parallel to the magnetic field (top) and perpendicular (bottom). The different lines mark the different states, as labeled. All distributions are calculated when the mean-squared displacement is equal to $10a^2$.

in the skeleton of the gel are almost permanently caged, while those in the surface or *skin* can escape more easily and diffuse over large distances. In the MR fluid studied here, however, these two populations are not present, as concluded from the distribution of displacements having only one peak shown in Fig. 11 for both directions parallel and perpendicular to the external field. The distributions are calculated for every state when the mean particle displacement in the coordinate is equal to $10a^2$.

IV. CONCLUSIONS

Using simulations, we have studied in this paper the equilibrium behavior of magnetorheological fluids, for increasing values of the interaction strength (controlled experimentally by an external static magnetic field). We have studied, and correlated, the structure and dynamics, focusing on the latter. Upon increasing the interaction strength, the particles form elongated clusters aligned with the external field, forming thick columns for intense fields. Concomitantly, the dynamics of the system slows down significantly, showing two-step relaxation, with a separation between the microscopic short-time and the structural long-time dynamics.

The intrinsic anisotropy of the MR fluids imposes a distinct behavior of the dynamics. While the trapping in the direction of the external field is stronger than in the perpendicular direction, the wave-vector dependence of the density correlation function is rather involved. The second decay is fitted with a Kohlrausch stretched exponential for wave vectors parallel and perpendicular to the field. The amplitude is larger in the perpendicular case than in the parallel one, although the reverse trend is expected from single-particle motion, and oscillates with the structure factor. The relaxation time scale shows the hydrodynamic q^{-2} behavior at low q, and oscillates also with $S(q)$, although some differences have also been observed. A strong decoupling between self-particle motion and structural relaxation is noticed, particularly in the transversal plane.

The results shown above suggest that the dynamical slowing down, leading ultimately to the increase of the viscosity, shares many similarities with the critical slowing down in colloidal glasses or gels. The structural relaxation can be described with a stretched exponential, and the wave-vector dependence of the parameters indicates that the dynamical behavior is dictated by the structure of the system, as in physical glasses. In particular, given the structural heterogeneities and the low density, our system is closer to particle gels.

Our results, thus, point to an interpretation of the MR effect as an attractive glass or gel transition. This idea is also supported by the observations of cluster growth in MR fluids, which is also similar to that of aggregation in, e.g.,

screened charged colloids, the initial steps in gel formation. Our analysis, however, could not identify the gel point, i.e., the critical value of U_0. We hope this work will motivate further studies to explore this approach to the MR effect, in particular, adapting models from glass and gel transitions that confirm the type of transition.

ACKNOWLEDGMENTS

This work was supported by the Spanish Ministerio de Economía y Competitividad (MINECO) and ERDF, under Projects No. FIS-2015-69022-P, No. MAT-2016-78778-R, No. MAT-2013-44429-R, and No. PCIN-2015-051, and the Junta de Andalucía under Project No. P11-FQM-7074.

[1] J. de Vicente, D. J. Klingenberg, and R. Hidalgo-Álvarez, Soft Matter **7**, 3701 (2011).
[2] J. Rabinow, AIEE Trans. **67**, 1308 (1948).
[3] J. Rabinow, National Bureau of Standards Technical News Bulletin **32**, 54 (1948).
[4] J. Rabinow, U.S. Patent 2.575.360 (1951).
[5] D. J. Klingenberg, AIChE J. **47**, 246 (2001).
[6] M. Heine, J. de Vicente, and D. J. Klingenberg, Phys. Fluids **18**, 023301 (2006).
[7] B. N. Reinecke, J. W. Shan, K. K. Suabedissen, and A. S. Cherkasova, J. Appl. Phys. **104**, 023507 (2008).
[8] J. Liu, G. A. Flores, and R. Sheng, J. Magn. Magn. Mater. **225**, 209 (2001).
[9] W. Kordonski and D. Golini, J. Intell. Mater. Syst. Struct. **13**, 401 (2002).
[10] S. Jha and V. K. Jain, Int. J. Mach. Tool Manufact. **44**, 1019 (2004).
[11] W. I. Kordonski, A. B. Shorey, and M. Tricard, J. Fluids Eng. **128**, 20 (2006).
[12] F. Donado, J. L. Carrillo, and M. E. Mendoza, J. Phys.: Condens. Matter **14**, 2153 (2002).
[13] K. J. Solis and J. E. Martin, Appl. Phys. Lett. **97**, 034101 (2010).
[14] D. H. Read and J. E. Martin, Anal. Chem. **82**, 2150 (2010).
[15] D. H. Read and J. E. Martin, Adv. Funct. Mater. **20**, 1577 (2010).
[16] D. H. Read and J. E. Martin, Anal. Chem. **82**, 6969 (2010).
[17] D. J. Klingenberg, F. van Swol, and C. F. Zukoski, J. Chem. Phys. **91**, 7888 (1989).
[18] D. J. Klingenberg, F. van Swol, and C. F. Zukoski, J. Chem. Phys. **94**, 6160 (1991).
[19] G. L. Gulley and R. Tao, Phys. Rev. E: Stat. Phys., Plasmas, Fluids, Relat. **48**, 2744 (1993).
[20] G. L. Gulley and R. Tao, Phys. Rev. E: Stat. Phys., Plasmas, Fluids, Relat. **56**, 4328 (1997).
[21] K. D. Weiss, J. D. Carlson, and D. A. Nixon, J. Intel. Mat. Systems and Struct. **5**, 772 (1994).
[22] J. de Vicente, F. Vereda, J. P. Segovia-Gutirrez, M. P. Morales, and R. Hidalgo-Álvarez, J. Rheol. **54**, 1337 (2010).
[23] K. Binder, W. Kob, *Glassy Materials and Disordered Solids: An Introduction to their Statistical Mechanics* (World Scientific, Singapore, 2011).
[24] K. Dawson, G. Foffi, M. Fuchs, W. Götze, F. Sciortino, M. Sperl, P. Tartaglia, Th. Voigtmann, and E. Zaccarelli, Phys. Rev. E **63**, 011401 (2000).
[25] K. N. Pham, A. M. Puertas, J. Bergenholtz, S. U. Egelhaaf, A. Moussaid, P. N. Pusey, A. B. Schofield, M. E. Cates, M. Fuchs, and W. C. K. Poon, Science **296**, 104 (2002).
[26] E. Zaccarelli, J. Phys.: Condens. Matter **19**, 323101 (2007).
[27] E. Bianchi, J. Largo, P. Tartaglia, E. Zaccarelli, and F. Sciortino, Phys. Rev. Lett. **97**, 168301 (2006)
[28] E. Del Gado and W. Kob, Phys. Rev. Lett. **98**, 028303 (2007).
[29] R. Blaak, M. A. Miller, and J.-P. Hansen, Europhys. Lett. **78**, 26002 (2007).
[30] P. Ilg and E. Del Gado, Soft Matter **7**, 163 (2011).
[31] J. P. Segovia-Gutirrez, J. de Vicente, R. Hidalgo-Alvarez, and A. M. Puertas, Soft Matter **9**, 6970 (2013).
[32] W. Kob, C. Donati, S. J. Plimpton, P. H. Poole, and S. C. Glotzer, Phys. Rev. Lett. **79**, 2827 (1997).
[33] M. Mohebi, N. Jamasbi, and J. Liu, Phys. Rev. E **54**, 5407 (1996).
[34] W. Paul and D. Y. Yoon, Phys. Rev. E **52**, 2076 (1995).
[35] P. J. Steinhardt, D. R. Nelson, and M. Ronchetti, Phys. Rev. B **28**, 784 (1983).
[36] P. Domínguez-García, Sonia Melle, J. M. Pastor, and M. A. Rubio, Phys. Rev. E **76**, 051403 (2007).
[37] J. Faraudo, J. S. Andreu, and J. Camacho, Soft Matter **9**, 6654 (2013).
[38] R. Tao and J. M. Sun, Phys. Rev. Lett. **67**, 398 (1991).
[39] L. Zhou, W. Wen, and P. Sheng, Phys. Rev. Lett. **81**, 1509 (1998).
[40] U. Dassanayake, S. Fraden, and A. van Blaaderen, J. Chem. Phys. **112**, 3851 (2000).
[41] A. Yethiraj and A. van Blaaderen, Int. J. Modern Phys. B **16**, 2328 (2002).
[42] A. K. Agarwal and A. Yethiraj, Phys. Rev. Lett. **102**, 198301 (2009).
[43] T. Gleim, W. Kob, and K. Binder, Phys. Rev. Lett. **81**, 4404 (1998).
[44] L. Berthier and W. Kob, J. Phys.: Condens. Matter **19**, 205130 (2007).
[45] V. Trappe and P. Sandkühler, Curr. Opinion Colloid Interf. Sci. **8**, 494 (2004).
[46] F. Weysser, A. M. Puertas, M. Fuchs, and Th. Voigtmann, Phys. Rev. E **82**, 011504 (2010)
[47] A. M. Puertas, M. Fuchs, and M. E. Cates, J. Chem. Phys. **121**, 2813 (2004).